J. Fluid Mech. (1990), *vol.* 220, *pp.* 161–186
Printed in Great Britain

The effects of surfactants on drop deformation and breakup

By H. A. STONE[1] AND L. G. LEAL[2]

[1] Division of Applied Sciences, Harvard University, Cambridge, MA 02138, USA

[2] Department of Chemical & Nuclear Engineering, University of California at Santa Barbara, Santa Barbara, CA 93106, USA

(Received 7 November 1989)

The effects of surface-active agents on drop deformation and breakup in extensional flows at low Reynolds numbers are described. In this free-boundary problem, determination of the interfacial velocity requires knowledge of the distribution of surfactant, which, in turn, requires knowledge of the interfacial velocity field. We account for this explicit coupling of the unknown drop shape and the evolving surfactant distribution. An analytical result valid for nearly spherical distortions is presented first. Finite drop deformation is studied numerically using the boundary-integral method in conjunction with the time-dependent convective–diffusion equation for surfactant transport. This procedure accurately follows interfacial tension variations, produced by non-uniform surfactant distribution, on the evolving interface. The numerical method allows for an arbitrary equation of state relating interfacial tension to the local concentration of surfactant, although calculations are presented only for the common linear equation of state. Also, only the case of insoluble surfactant is studied.

The analytical and numerical results indicate that at low capillary numbers the presence of surfactant causes larger deformation than would occur for a drop with a constant interfacial tension equal to the initial equilibrium value. The increased deformation occurs owing to surfactant being swept to the end of the drop where it acts to locally lower the interfacial tension, which therefore requires increased deformation to satisfy the normal stress balance. However, at larger capillary numbers and finite deformations, this convective effect competes with 'dilution' of the surfactant due to interfacial area increases. These two different effects of surface-active material are illustrated and discussed and their influence on the critical capillary number for breakup is presented.

1. Introduction

It is well-established that interfacial tension variations and/or interfacial viscosity and elasticity can have dramatic qualitative and quantitative effects on free-surface flows (Levich & Krylov 1969). For example, the drag on a small fluid sphere obeys Stokes law rather than the ideal Hadamard–Rybczynski result in all but very clean systems, bubbles are observed to migrate in a temperature gradient, and ocean waves may be damped by a thin oil film. Furthermore, it is clear that the effects of surfactants must be properly understood if the results of fundamental (model) problems are to be useful in real engineering applications. In this paper, we study the effect of interfacial tension variations, due to surface-active agents, on the deformation and breakup of Newtonian drops in straining flows.

There have been many previous studies concerned with the effect of surfactants on buoyancy-driven motion of drops and bubbles in quiescent fluids. For example, it is observed that even a small amount of surfactant can reduce the terminal velocity of drops and reduce the rate of solute transport to or from drops. A valuable compendium related to this topic is the classic treatise on *Physicochemical Hydrodynamics* by Levich (1962). Additional theoretical analyses of different aspects of the translating drop problem have been discussed by Newman (1967), Haber & Hetsroni (1971), Saville (1973), LeVan & Newman (1976), and Holbrook & LeVan (1983*a*, *b*). A common assumption in all of these studies is that the drop remains spherical. The small, flow-induced steady deformation of a translating drop has been calculated by Sadhal & Johnson (1986).

A major interest in our laboratory is the deformation and breakup of droplets due to extensional flows. This topic stems from G. I. Taylor's classical experimental and theoretical studies (1932, 1934) that were motivated by an interest in emulsion formation. Much work has been performed in the interim, focusing mainly on drop deformation in the absence of interfacial tension gradients. For example, a number of authors have reported theoretical analyses for drop shapes in the near-sphere limit, and in the absence of interfacial tension gradients, e.g. Cox (1969) and Barthes-Biesel & Acrivos (1973). Numerical work has been reported by Rallison & Acrivos (1978), among others, on finite deformation in the absence of interfacial tension gradients. Related experimental studies are discussed by Mason & coworkers (e.g. Rumscheidt & Mason 1961 and Torza, Cox & Mason 1972) and Bentley & Leal (1986). Two review articles describing much of this work have been written by Acrivos (1983) and Rallison (1984).

More recently, we have undertaken a new comprehensive experimental and theoretical investigation of drop breakup at low Reynolds number under a wider range of flow conditions, but again in the absence of interfacial tension gradients (Stone, Bentley & Leal 1986 and Stone & Leal 1989). In all cases, interfacial tension effects play a critical role, and in many cases the breakup process is a consequence of interfacial-tension-driven motions due to curvature variations along the surface. An obvious question is how these phenomena are affected by Marangoni effects associated with surface tension gradients along the interface, or possibly by other interfacial properties such as surface viscosity.

Unfortunately, the theoretical problem of finite drop deformation, incorporating dynamic interfacial properties, has received very little attention in the literature. To our knowledge, the only theoretical study that addresses the question of drop deformation in shear-type flows is due to Flumerfelt (1980). Flumerfelt examined the deformation and orientation of nearly spherical drops in simple shear and extensional flows, incorporating interfacial tension variations as well as effects due to surface shear and dilatational viscosity. Related experiments in simple shear flow are reported by Phillips, Graves & Flumerfelt (1980). However, because the work of Flumerfelt and coworkers is restricted to small deformations, it is difficult to extract information about drop breakup. Additional experiments reporting some qualitative observations of drop deformation in the presence of surfactants are reported by Smith & van de Ven (1985).

This paper is concerned with finite deformation and breakup of drops, *including* interfacial tension gradients produced by non-uniform concentration of a surfactant. The great difficulty in treating this free-boundary problem stems from the *a priori* unknown location of the fluid–fluid interface. The presence of surfactants complicates matters further because their distribution is intimately coupled to the drop shape

and interface mobility, which in turn affect the time-dependent evolution of the drop shape. We first outline an analytical result valid for small drop deformations. Then, in order to study finite deformations, a numerical procedure based upon the boundary-integral method is described. This combined analytical and numerical study leads to improved physical insight into the effects of surfactants on drop dynamics in situations where finite deformation is important.

It is interesting to note that dynamical effects and fluid motions produced by interfacial tension gradients have proven useful in fluid mechanical modelling of cell division and cell motion. Greenspan (1978) provides a vivid experimental illustration of drop breakup caused by surface tension variations along the interface, produced by the deliberate addition of a surfactant. Recently, Zinemanas & Nir (1988) discussed a more complete cell cleavage model incorporating active elements transported along the fluid interface and used a numerical procedure similar to the one reported here.

2. Problem statement

Consider a neutrally buoyant Newtonian liquid droplet of undeformed radius a, and viscosity $\hat{\mu}$, suspended in a second immiscible Newtonian fluid with viscosity μ. Far from the drop the continuous phase undergoes a prescribed linear flow characterized by the shear rate G. The fluids are isothermal. The fluid–fluid interface is assumed to be characterized completely by the interfacial tension σ and all stresses associated with the rate of deformation of the interface (i.e. surface shear and dilatational viscosity) are neglected. The interfacial tension, though, may vary with position along the interface owing to the presence of adsorbed surface-active material. The surfactant is assumed to be insoluble in either the droplet fluid or the suspending fluid so that convection and diffusion of surfactant in the bulk phases may be neglected. The case of insoluble surfactant corresponds to the physical situation where the surfactant has such an extremely low solubility in either of the bulk phases that it may be assumed to reside only at the fluid–fluid interface. Therefore, with the exception of σ, all fluid properties are treated as constants.

We begin by assuming that the Reynolds numbers characterizing motion in both fluids are small so that inertia may be neglected completely and the quasi-steady Stokes equations apply for both fluid phases. This common low-Reynolds-number assumption is valid for the small drops typical of many industrial applications. In order to non-dimensionalize the governing equations and boundary conditions, we use the undeformed drop radius, a, as a characteristic lengthscale, the product Ga as a characteristic velocity, characteristic pressures for the drop and continuous phases are defined as $\hat{\mu}G$ and μG, respectively, and a characteristic timescale is G^{-1}. The governing equations for the velocity and pressure fields $(\boldsymbol{u}, p)$ in the suspending fluid and in the droplet fluid $(\hat{\boldsymbol{u}}, \hat{p})$ are

$$\left.\begin{aligned} \nabla^2 \boldsymbol{u} = \nabla p, \quad \nabla^2 \hat{\boldsymbol{u}} = \nabla \hat{p}, \\ \nabla \cdot \boldsymbol{u} = 0, \quad \nabla \cdot \hat{\boldsymbol{u}} = 0. \end{aligned}\right\} \tag{1}$$

Relative to a coordinate system fixed to the centre of mass of the drop, the velocity field at large distances from the drop is taken to be a linear flow, $\boldsymbol{u}_\infty = \frac{1}{2}\boldsymbol{\omega} \wedge \boldsymbol{x} + \boldsymbol{E} \cdot \boldsymbol{x}$. $\boldsymbol{\omega}$ and $\boldsymbol{E}$ are the vorticity vector and rate-of-strain tensor, respectively, for the undisturbed flow. Although the small-deformation theory discussed in §3 applies to this general flow situation, most calculations in this paper are restricted to the axisymmetric extensional flow

$$\boldsymbol{u} \to \boldsymbol{u}_\infty(\boldsymbol{x}) = \pm \begin{pmatrix} -\frac{1}{2} & 0 & 0 \\ 0 & -\frac{1}{2} & 0 \\ 0 & 0 & 1 \end{pmatrix} \cdot \boldsymbol{x} \quad \text{as} \quad |\boldsymbol{x}| \to \infty, \tag{2}$$

where the + sign corresponds to a uniaxial extensional flow and the − sign corresponds to a biaxial extensional flow.

The interfacial tension σ depends on the surface concentration Γ^* of surfactant, which generally acts to lower the interfacial tension, and is given by an equation of state of the form

$$\sigma = \sigma(\Gamma^*). \tag{3}$$

The surface concentration Γ^* is specified in units of mass of surfactant per unit of interfacial area. If the surfactant is present in dilute concentrations, then a linear relationship exists between σ and Γ^*, in which case (3) is typically written as (Adamson 1976)

$$\sigma_s - \sigma = \pi = \Gamma^* RT, \tag{4}$$

where π is known as the 'spreading pressure', R is the gas constant, T is the absolute temperature and σ_s is the interfacial tension of the clean interface (pure solvent). This simple equation of state has been used widely by previous researchers for examining the effects of interfacial tension gradients on the drag and interface mobility of rising drops, etc. Because of the form of this equation, (4) is often called the two-dimensional gas law. Other relations between σ and Γ^* are possible. For example, in order to account for non-ideality (e.g. the finite area occupied by the surfactant molecules in addition to intermolecular forces), versions of (4) similar to the well-known van der Waals equation of state are written as

$$\left(\pi + \frac{v}{A^2}\right)(A - A^0) = RT, \tag{5}$$

where A represents the area per molecule, $A = 1/\Gamma^*$, A^0 is the excluded area per molecule and v accounts for the attraction between surfactant molecules (Adamson 1976). Clearly, the more complicated the equation of state, the more parameters are necessary to completely specify the problem. Therefore, we restrict ourselves to the linear equation (4).

To complete the problem formulation, we require boundary conditions at the interface. For the velocity field, these conditions are continuity of velocity

$$\boldsymbol{u} = \hat{\boldsymbol{u}} \quad \text{for} \quad \boldsymbol{x}_s \in S, \tag{6}$$

the kinematic condition

$$\frac{\mathrm{d}\boldsymbol{x}_s}{\mathrm{d}t} = \boldsymbol{n}(\boldsymbol{u} \cdot \boldsymbol{n}), \tag{7}$$

and the stress balance, which may be written in the dimensionless form

$$\boldsymbol{n} \cdot \boldsymbol{T} - \lambda \boldsymbol{n} \cdot \hat{\boldsymbol{T}} = \frac{\sigma}{\mu G a} \boldsymbol{n}(\nabla_s \cdot \boldsymbol{n}) - \frac{1}{\mu G a} \nabla_s \sigma \quad \text{for} \quad \boldsymbol{x}_s \in S. \tag{8}$$

In these equations, $\boldsymbol{T}$ is the stress tensor, $\boldsymbol{x}_s$ represents a point on the fluid–fluid interface S, $\boldsymbol{n}$ is the unit outward normal directed from the droplet phase to the continuous phase (see figure 1), $\nabla_s \cdot \boldsymbol{n}$ is the mean curvature of the interface, ∇_s is the

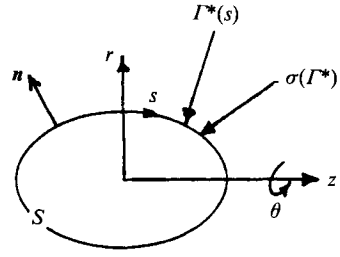

FIGURE 1. Schematic of the problem and definition of variables.

surface gradient operator ($\nabla_s = (\boldsymbol{I}-\boldsymbol{nn})\cdot\nabla$) and $\lambda = \hat{\mu}/\mu$ denotes the viscosity ratio of the two fluids. The interfacial tension σ is given by (4), with the surface concentration non-dimensionalized using the uniform concentration Γ_0, which exists on the interface in the absence of any flow. Letting $\Gamma = \Gamma^*/\Gamma_0$, equations (4) and (8) lead to

$$\boldsymbol{n}\cdot\boldsymbol{T}-\lambda\boldsymbol{n}\cdot\hat{\boldsymbol{T}} = \frac{(1-\beta\Gamma)}{\mathbb{C}_s}\boldsymbol{n}(\nabla_s\cdot\boldsymbol{n})+\frac{\beta}{\mathbb{C}_s}\nabla_s\Gamma \quad \text{for} \quad \boldsymbol{x}_s\in S. \tag{9}$$

Here we have introduced $\mathbb{C}_s = \mu Ga/\sigma_s$ and $\beta = \Gamma_0 RT/\sigma_s$. $\mathbb{C}_s$ is the capillary number based upon the interfacial tension for an uncontaminated interface and β is a physicochemical parameter that determines the sensitivity of the interfacial tension to changes in surfactant concentration. The capillary number $\mathbb{C}_s$ is the appropriate dimensionless measure of viscous forces relative to interfacial tension forces based upon the interfacial tension σ_s for the clean interface without surfactant. The interfacial tension with surfactant present is $\sigma_s(1-\beta\Gamma)$, so that

$$\frac{\mathrm{d}(\sigma/\sigma_s)}{\mathrm{d}\Gamma} = -\beta. \tag{10}$$

Hence, in the absence of flow, the uniform surfactant concentration Γ_0 decreases the surface tension to $\sigma^* = \sigma_s(1-\beta)$. This shows that β is bounded by $0 \leqslant \beta \leqslant 1$. Further, it suggests that it may be useful to consider the capillary number based upon the equilibrium interfacial tension σ^* rather than σ_s. This capillary number is denoted $\mathbb{C}^*$ where $\mathbb{C}^* = \mathbb{C}_s/(1-\beta)$.

In assessing the influence of surfactant in the present problem, there are two baseline cases to consider. The first point of view is to compare all results with the behaviour of the same drop but with an uncontaminated interface. In this case, the dominant effect of surfactant in most instances is to decrease the interfacial tension from σ_s to σ^* with the influence of fluid motion leading to values above or below σ^* depending on the surfactant concentration Γ, which lies in the range $0 \leqslant \Gamma \leqslant \beta^{-1}$ (the upper limit represents $\sigma = 0$). The alternative point of view is to compare the results accounting for interfacial tension gradients with the results that would be obtained for the same drop but with an interfacial tension that remains constant at the value $\sigma_s(1-\beta)$, which represents the uniformly contaminated surface at the initial equilibrium concentration, $\Gamma = 1$. From an experimental standpoint, the latter description is perhaps the most natural one. For example, in order to predict the behaviour of a two-fluid system, one would measure the equilibrium value for the interfacial tension (without any consideration of interface contamination), and then use this value together with the critical capillary number for a clean system to predict the critical flow conditions for breakup. Within this framework, it is only the

differences in the critical capillary number produced by flow-induced surfactant concentration changes that one would need to be concerned with.

In this paper, we adopt the latter point of view. Thus, we express all results in terms of the capillary number $\mathbb{C}^*$ based upon $\sigma^* = \sigma_s(1-\beta)$. It is important to remember that the reduction in interfacial tension from σ_s to σ^* is thereby built in to the description of surfactant effects.

Using the uniformly contaminated interface as the reference state, it is convenient to express Γ as

$$\Gamma = 1 + \Gamma', \tag{11}$$

so that Γ' represents the local deviation of surfactant concentration from the uniformly coated interface. Substituting (11) into (9), we then obtain the stress balance in the form

$$\boldsymbol{n}\cdot\boldsymbol{T} - \lambda\boldsymbol{n}\cdot\hat{\boldsymbol{T}} = \frac{1}{\mathbb{C}^*}\boldsymbol{n}(\nabla_s\cdot\boldsymbol{n}) - \frac{\beta}{\mathbb{C}^*(1-\beta)}[\Gamma'\boldsymbol{n}(\nabla_s\cdot\boldsymbol{n}) - \nabla_s\Gamma'] \quad \text{for} \quad \boldsymbol{x}_s \in S. \tag{12}$$

The first term on the right-hand side of (12) is the usual capillary contribution to the normal stress balance based upon the effective capillary number $\mathbb{C}^* = \mathbb{C}_s/(1-\beta)$. The last two terms on the right-hand side of (12) represent the effects of flow-induced changes in surfactant concentration. The first of these appears in the normal stress balance and, crudely speaking, may be thought of as a direct influence on drop shape due to the variation of interfacial tension from its original uniform value. The second term in brackets in (12) appears in the tangential stress balance and is the Marangoni contribution to this problem.

From (12) we may conclude that changes in drop shape as a result of changes in surfactant concentration may be neglected if

$$\frac{\beta|\Gamma'|}{(1-\beta)} \ll 1. \tag{13}$$

On the other hand, the Marangoni contribution to (12) cannot generally be neglected unless

$$\frac{\beta|\Gamma'|}{\mathbb{C}^*(1-\beta)} \ll 1, \tag{14}$$

which is much more restrictive than (13) for the small capillary numbers studied here. Of course, (14) assumes that the characteristic lengthscale remains a, an assumption that is likely to break down when large local gradients in Γ occur (i.e. large Péclet numbers; see (16)) or the drop becomes highly deformed.

We have already noted that the interface mobility and the flow-induced changes in the drop shape will lead to a non-uniform distribution of surfactant along the interface. The changes in surfactant concentration at a phase interface are governed by a time-dependent convective–diffusion equation that may be written in the dimensionless form (Aris 1962; Waxman 1984; Stone 1990)

$$\frac{\partial\Gamma}{\partial t} + \nabla_s\cdot\left[\Gamma\boldsymbol{u}_s - \frac{1}{P_s}\nabla_s\Gamma\right] + \Gamma(\nabla_s\cdot\boldsymbol{n})(\boldsymbol{u}\cdot\boldsymbol{n}) = j_n. \tag{15}$$

Here, $\boldsymbol{u}_s$ represents the velocity vector tangent to the interface ($\boldsymbol{u}_s = (\boldsymbol{I}-\boldsymbol{nn})\cdot\boldsymbol{u}$) and j_n represents the dimensionless net flux of surface-active material to and from the interface from either of the bulk phases. For the case of insoluble surfactant to be

studied here, $j_n = 0$. The importance of convection relative to diffusion is measured by a surface Péclet number

$$P_s = \frac{Ga^2}{\mathscr{D}_s}, \tag{16}$$

where $\mathscr{D}_s$ is the surface diffusivity. The fourth term in (15) is a source-like contribution to the surface convective–diffusion equation that accounts for changes in the local surface concentration due to stretching and distortion of the interface (i.e. the total interfacial area changes as the drop deforms) and appears simply as the product of the normal velocity and the local curvature.

For some physical situations it is convenient to consider changes in drop shape produced solely by increases in the local shear rate G. In such instances, rather than choosing $\mathbb{C}^*$ and P_s as the independent dimensionless parameters, it is useful to define

$$\gamma = \frac{\sigma^* a}{\mu \mathscr{D}_s} \tag{17}$$

so that $P_s = \gamma \mathbb{C}^*$ and γ depends on material properties only (γ appears analogous in some ways to a Prandtl number). Then, drop deformation is solely a function of the dimensionless shear rate $\mathbb{C}^*$ for a given constant γ and β.

Thus, finally, the problem is to solve equations (1) subject to conditions (6), (7), (12) and (15). These equations clearly indicate the difficulty in solving problems where surface-active agents are important. Determination of the interfacial velocity field requires knowledge of the distribution of surfactant which, in turn, necessitates knowledge of the interfacial velocity field. The free-boundary character of this problem is an additional non-trivial complication as the interface location is *a priori* unknown and must be found as part of the solution to the problem.

In this paper, we consider an initially spherical drop with uniformly distributed surfactant, concentration Γ_0 (i.e. a dimensionless initial concentration $\Gamma = 1$), in an extensional flow. Our goal is to understand the coupled effects of $\mathbb{C}^*$ (or $\mathbb{C}_s$), γ (or P_s) and β. In the next section, we briefly consider the small deformation of a drop, including interfacial tension variations associated with surfactant gradients caused by the flow. Following this, we consider numerical calculations based upon the boundary-integral technique for finite deformations. As discussed by Rallison (1981), calculations with $\lambda = 1.0$ are much simpler than other values of λ, but still provide qualitative insight into the behaviour for most viscosity ratios. Thus, we limit our numerical calculations in this paper to $\lambda = 1.0$. The numerical method for solving this problem is outlined in §4.

Finally, for the modest deformations studied in this paper, the degree of drop deformation is characterized using the deformation parameter $D = (L-B)/(L+B)$, where L and B represent the half-length and half-breadth of the drop, respectively.

3. Small-deformation analysis

In this section we summarize analytical results for the small deformation of a drop, accounting for surfactant effects. The results are useful both as a check on the numerical calculations and as a guide to physical insight into the initial effects of surfactants. The analysis is similar to the work of Flumerfelt (1980) who considered surface shear and dilatational viscosity, as well as interfacial tension variations, including mass transfer from the bulk but neglecting surface diffusion (limit $P_s \to \infty$). Here we only consider gradients in σ, allow for surface diffusion of surfactant

(although analytical results are restricted to small surface Péclet numbers), but neglect interphase mass transfer. The analysis follows well-known small-deformation studies for nearly spherical drops (e.g. Cox 1969) so we simply summarize the important results for this study.

Both the drop radius and surfactant concentration are assumed to be only slightly perturbed from their equilibrium values. For a linear flow field generated by a second-order tensor, the first corrections to the description of the surface shape and the nearly uniform surfactant distribution are also expected to be described by second-order tensors, which may be taken, without loss of generality, to be proportional to $\boldsymbol{E}$. So,

$$r = 1 + \mathbb{C}^* b_r(t) \frac{\boldsymbol{x}\cdot\boldsymbol{E}\cdot\boldsymbol{x}}{r^2} \tag{18a}$$

$$\Gamma = 1 + \gamma\mathbb{C}^* b_\Gamma(t) \frac{\boldsymbol{x}\cdot\boldsymbol{E}\cdot\boldsymbol{x}}{r^2}. \tag{18b}$$

The coefficients $b_r(t)$ and $b_\Gamma(t)$ describe the time-evolution of the shape and surfactant distributions. The dependencies on $\mathbb{C}^*$ and $P_s = \gamma\mathbb{C}^*$ follow from analysis of the normal stress balance (e.g. equation (12)) and the surface convective–diffusion equation, respectively. Details of the small-deformation analysis, including determination of the velocity field, are given in the Appendix. The analysis assumes that $\mathbb{C}^* \ll 1$, $\gamma = O(1)$ ($P_s \ll 1$) and $\lambda = O(1)$. Also, it may be noted that here the precise form of the constitutive equation (4) does not matter, but rather, for the nearly uniform surfactant distributions assumed in this analytical approximation, only the linearized version of the constitutive equation is relevant. We find that the steady-state solution for the drop deformation is given by

$$b_r = \frac{5}{4}\frac{(16+19\lambda)+4\beta\gamma/(1-\beta)}{10(1+\lambda)+2\beta\gamma/(1-\beta)}, \tag{19}$$

so that the deformation parameter D describing the small deviations from a spherical shape is

$$D \approx \frac{3\mathbb{C}^* b_r}{4+\mathbb{C}^* b_r}. \tag{20}$$

Also, the steady surfactant distribution is given by

$$b_\Gamma = \frac{5}{10(1+\lambda)+2\beta\gamma/(1-\beta)}. \tag{21}$$

Clearly, (19) reduces to the classical Taylor result in the limits $\beta \to 0$ or $\gamma \to 0$. These limits correspond, respectively, to the physical situations where either there is no effect of surfactant on the interfacial tension or where surfactant gradients do not arise, because the surface concentration is dominated by diffusion.

We note that the drop deformation increases as the magnitude of b_r increases. Hence, for a given linear flow, the deformation increases if either γ (or P_s) or β is increased at a fixed dimensionless shear rate $\mathbb{C}^*$. For the small-deformation analysis, the effect of surfactant convection appears via the combined parameter $\beta\gamma/(1-\beta)$, which is proportional to the magnitude of the interfacial tension variations at this order of approximation. The physical mechanism for the increase in deformation is that the flow convects surfactant toward the end of the drop, resulting in a higher

surfactant concentration and lower interfacial tension. This, in turn, requires larger deformations to balance viscous forces. It is perhaps worthwhile to repeat the statement that this increase in deformation is relative to the drop shape with uniform surfactant concentration, $\Gamma = 1$. Drop deformation would also increase, at a fixed shear rate G, owing to the decrease in interfacial tension from the clean surface value σ_s to the equilibrium value $\sigma^* = \sigma_s(1-\beta)$, but this is incorporated into the definition of the capillary number $\mathbb{C}^*$. Equation (20) will be compared with numerical solutions in §5 (figure 3) and we shall see that this mechanism for increased deformation remains dominant even in some of the finite-deformation cases.

We also note that the time-dependent evolution of nearly spherical drops in steady linear flows can be calculated as shown in the Appendix. A second-order ordinary differential equation with constant coefficients is obtained for $b_r(t)$:

$$\frac{(2\lambda+3)(16+19\lambda)(1-\beta)}{2\beta}\mathbb{C}^{*2}\frac{\mathrm{d}^2 b_r}{\mathrm{d}t^2} + \left[\frac{3(2\lambda+3)(16+19\lambda)(1-\beta)\mathbb{C}^*}{\beta\gamma} + \frac{20}{\beta}(1+\lambda)(1-\beta)\mathbb{C}^* + (32+23\lambda)\mathbb{C}^*\right]\frac{\mathrm{d}b_r}{\mathrm{d}t} + 12\left[\frac{10(1+\lambda)}{\beta\gamma}(1-\beta)+2\right]b_r = 15\left[\frac{(16+19\lambda)}{\beta\gamma}(1-\beta)+4\right]. \quad (22)$$

A similar equation is found for $b_I(t)$. It can be shown that the characteristic equation derived from (22) has two real negative roots. Hence, beginning with a spherical drop and uniformly distributed surfactant, we find that both the drop shape and surfactant distribution monotonically approach the final steady state at an exponential rate. In particular, there are no oscillations and, clearly, the (two) characteristic rate constants are dependent on both the characteristic dimensionless deformation timescale ($\mathbb{C}^*$) and the dimensionless convective–diffusion timescale ($\gamma\mathbb{C}^* = P_s$). However, because these time-dependent results are limited to almost spherical distortions, the practical utility of the quantitative details in (22) are limited.

4. Numerical method/implementation

The analysis summarized in the preceding section is limited to small deformations from the spherical state. In this section, we discuss a numerical procedure to solve the coupled free-boundary and surface transport problem for moderate and large deformations.

In §4.1 we describe the calculation of the interfacial velocity and outline the procedure used to discretize and represent the drop surface. The surfactant convective–diffusion equation is examined in detail in §4.2 and is simplified to a form suitable for this axisymmetric problem. The coupling of the unknown drop shape and the evolving surfactant distribution makes solution of the simultaneous system of equations extremely difficult, so in §4.3 we outline an approximate procedure for solving the problem.

4.1. *Calculation of the surface velocity using the boundary-integral method*

The boundary-integral method is an efficient technique for solving Stokes flow problems. It is particularly well suited for free-boundary studies since only the boundary of the domain must be discretized and the interfacial velocity is calculated

directly. The first application of the boundary-integral method to studies of droplet deformation was described by Rallison & Acrivos (1978) and, since that time, the technique has been used by many investigators for a wide range of free-boundary studies. For example, in our research group the motion of a sphere normal to a deformable fluid–fluid interface has been discussed by Lee & Leal (1982) and Stoos & Leal (1989), and the mechanism of drop breakup has been investigated by Stone & Leal (1989). Also, the method has been applied to drop deformation and breakup in electric and magnetic fields by Sherwood (1988) and to problems of cell deformation by Li, Barthes-Biesel & Helmy (1988) and Zinemanas & Nir (1988). An investigation related to the work reported here is the numerical study by Ascoli & Leal (1990) of drop migration normal to a solid planar wall due to a temperature gradient.

Following the procedure of Rallison & Acrivos (1978) and making use of the stress boundary condition (9), the interfacial velocity $\boldsymbol{u}(\boldsymbol{x}_s)$ can be written as

$$\tfrac{1}{2}(1+\lambda)\,\boldsymbol{u}(\boldsymbol{x}_s) = \boldsymbol{u}_\infty(\boldsymbol{x}_s) - \int_S \boldsymbol{J}\cdot\left[\frac{(1-\beta\Gamma)}{\mathbb{C}^*(1-\beta)}\boldsymbol{n}(\nabla_s\cdot\boldsymbol{n}) + \frac{\beta}{\mathbb{C}^*(1-\beta)}\nabla_s\Gamma\right]\mathrm{d}S(\boldsymbol{y}) - (1-\lambda)\int_S \boldsymbol{n}\cdot\boldsymbol{K}\cdot\boldsymbol{u}\,\mathrm{d}S(\boldsymbol{y}), \quad (23)$$

where $\boldsymbol{J} = \frac{1}{8\pi}\left[\frac{\boldsymbol{I}}{|\boldsymbol{x}_s-\boldsymbol{y}|} + \frac{(\boldsymbol{x}_s-\boldsymbol{y})(\boldsymbol{x}_s-\boldsymbol{y})}{|\boldsymbol{x}_s-\boldsymbol{y}|^3}\right]$, $\boldsymbol{K} = -\frac{3}{4\pi}\frac{(\boldsymbol{x}_s-\boldsymbol{y})(\boldsymbol{x}_s-\boldsymbol{y})(\boldsymbol{x}_s-\boldsymbol{y})}{|\boldsymbol{x}_s-\boldsymbol{y}|^5}$.

Here $\boldsymbol{y}$ is the integration variable and $\boldsymbol{u}_\infty$ is given by (2).

This integral equation of the second kind highlights the principal advantage of the boundary-integral method, namely that it is only necessary to compute two-dimensional surface integrals rather than performing calculations over the entire three-dimensional fluid domain. Once the interfacial velocity is determined the drop shape can be updated using the kinematic condition. Clearly, the surfactant contribution to the problem directly enters (23) only through β. It should be recalled, however, that the capillary number $\mathbb{C}^*$, which we treat as an independent parameter, also contains implicitly the decrease in interfacial tension from σ_s to $\sigma_s(1-\beta)$ due to the addition of surfactant. More general equations of state other than the linear form (4) alter equation (23) only slightly. Hence, once an equation of state is chosen, the solution of (23) is no more difficult for more complicated equations of state. However, in this study, we shall only examine the linear relation discussed in §2.

The solution of this integral equation for the interfacial velocity must be accomplished numerically. The approach taken is to first discretize the interface, write the integral equation at each node point and reduce (23) to an equivalent set of linear algebraic equations that is straightforward to solve using Gaussian elimination. Assuming for the moment that the surface concentration Γ and drop shape are known, there are three important aspects necessary for an accurate numerical solution of this integral equation: (i) the geometry must be accurately represented so that the interface curvature, which involves second derivatives, can be computed; (ii) the functional representation must be chosen for the variation of the unknown velocity field $\boldsymbol{u}(\boldsymbol{x}_s)$ over each surface element; and (iii) accurate evaluation of integrals is required, including careful resolution near the singular points $\boldsymbol{y}\to\boldsymbol{x}_s$ where the kernels $\boldsymbol{J}$ and $\boldsymbol{K}$ are singular, although the integrals themselves are integrable in the sense of a Cauchy principal value.

We have dealt with the above difficulties in a previous investigation of the breakup of highly elongated droplets (Stone & Leal 1989). The results of that study give us confidence that the numerical aspects of the problem are well resolved. Here we simply summarize our approach.

We only consider axisymmetric drop shapes. Referring to the cylindrical coordinate system shown in figure 1, the azimuthal integration in (23) can be performed analytically. This reduces the surface integrals to line integrals. Then, the interface is discretized into $2N-2$ boundary elements with node points placed at the end of each element, and $\boldsymbol{u}(\boldsymbol{x}_s)$ is assumed to vary linearly over each element. At each node point there are two unknown components of the interfacial velocity vector (u_r, u_z). The interface location is parametrized using a normalized measure of arclength s ($0 \leqslant s \leqslant 1$). In this case, the surface collocation points are labelled using cylindrical coordinates (r, z) and cubic splines are used to generate twice continuously differentiable representations for $r = r(s)$ and $z = z(s)$. These cubic spline representations are used to calculate the unit normal $\boldsymbol{n}$ and the curvature $\nabla_s \cdot \boldsymbol{n}$ along the interface. Finally, because of the fore–aft symmetry of the flow fields, the drop shapes and the surfactant distributions considered for the numerical aspects of this paper, the number of unknowns in the linearized form of (23) is halved and a $2N-2$ system of equations and unknowns is solved using Gaussian elimination. However, the calculations reported in this paper are for $\lambda = 1$ only, which is considerably simpler as no matrix inversion is required.

4.2. *Calculation of the surfactant distribution*

We first make some general remarks concerning the general form of the convective–diffusion equation (15) appropriate for a two-dimensional surface imbedded in a three-dimensional space. Time-dependent effects are also incorporated, including changes in drop shape. In general, the two-dimensional surface can be represented by $\boldsymbol{x}_s = \boldsymbol{x}_s(v^1, v^2, t)$, where the v^α represent coordinates fixed in the surface. For a discussion of the differential geometry of surface coordinates the reader is referred to McConnell (1957), Aris (1962) and Waxman (1984). The convection term in (15) can be written using index notation and the summation convention as

$$\nabla_s \cdot (\Gamma \boldsymbol{u}_s) = \frac{1}{\bar{a}^{\frac{1}{2}}} \frac{\partial}{\partial v^\alpha} (\Gamma \bar{a}^{\frac{1}{2}} u^\alpha), \tag{24}$$

where the surface velocity $\boldsymbol{u}_s$ is defined with respect to the surface base vectors $\boldsymbol{a}_\alpha$ as

$$\boldsymbol{u}_s = u^\alpha \boldsymbol{a}_\alpha, \quad \boldsymbol{a}_\alpha = \frac{\partial \boldsymbol{x}_s}{\partial v^\alpha} \quad (\alpha = 1, 2) \tag{25}$$

and $\bar{a}$ is the determinant of the surface metric tensor. A differential element of surface is related to $\bar{a}$ and differential changes in the surface coordinates by

$$\mathrm{d}S = \bar{a}^{\frac{1}{2}} \mathrm{d}v^1 \, \mathrm{d}v^2. \tag{26}$$

The surface Laplacian can be written as

$$\nabla_s^2 \Gamma = \frac{1}{\bar{a}^{\frac{1}{2}}} \frac{\partial}{\partial v^\alpha} \left(\bar{a}^{\frac{1}{2}} a^{\alpha\beta} \frac{\partial \Gamma}{\partial v^\beta} \right), \tag{27}$$

where $a^{\alpha\beta}$ are the surface covariant components of the surface metric tensor.

Using the above relationships the convective–diffusion equation (15) may then be written in the more compact form

$$\frac{\partial \Gamma}{\partial t}+\frac{1}{\bar{a}^{\frac{1}{2}}}\frac{\partial}{\partial v^{\alpha}}(\Gamma \bar{a}^{\frac{1}{2}}u^{\alpha})-\frac{1}{P_{\mathrm{s}}\bar{a}^{\frac{1}{2}}}\frac{\partial}{\partial v^{\alpha}}\left(\bar{a}^{\frac{1}{2}}a^{\alpha\beta}\frac{\partial \Gamma}{\partial v^{\beta}}\right)+\Gamma(\nabla_{\mathrm{s}}\cdot \boldsymbol{n})\,(\boldsymbol{u}\cdot \boldsymbol{n})=0. \tag{28}$$

A similar development has been discussed by Zinemanas & Nir (1988) in a numerical study of cell deformation.

In general the drop surface can be parametrized using the orthogonal surface coordinate system (s,θ) where θ is the azimuthal angle ($0\leqslant\theta\leqslant 2\pi$) and s is the normalized measure of arclength introduced in §4.1 (see figure 1). In this axisymmetric problem, (28) reduces to

$$\frac{\partial \Gamma}{\partial t}+\frac{1}{\bar{a}^{\frac{1}{2}}}\frac{\partial}{\partial s}(\Gamma \bar{a}^{\frac{1}{2}}u^{\mathrm{s}})-\frac{1}{P_{\mathrm{s}}\bar{a}^{\frac{1}{2}}}\frac{\partial}{\partial s}\left(\bar{a}^{\frac{1}{2}}a^{11}\frac{\partial \Gamma}{\partial s}\right)+\Gamma(\nabla_{\mathrm{s}}\cdot \boldsymbol{n})\,(\boldsymbol{u}\cdot \boldsymbol{n})=0. \tag{29}$$

The time-dependent metric $\bar{a}$ is given in cylindrical coordinates by

$$\bar{a}(s,t)=\det(a_{\alpha\beta})=r(s)^2\left[\left(\frac{\partial r}{\partial s}\right)^2+\left(\frac{\partial z}{\partial s}\right)^2\right]$$

and

$$a^{11}=\frac{1}{\left(\dfrac{\partial r}{\partial s}\right)^2+\left(\dfrac{\partial z}{\partial s}\right)^2}.$$

Since the surface base vectors $\boldsymbol{a}_{\alpha}$ are not in general unit vectors, the surface velocity u^{s} in (29) is related to the tangential velocity component $\boldsymbol{u}(\boldsymbol{x}_{\mathrm{s}})\cdot \boldsymbol{t}=\bar{u}^{\mathrm{s}}$ calculated using the boundary-integral technique described in §4.1 by ($\boldsymbol{t}$ denotes the unit tangent vector to the surface)

$$u^{\mathrm{s}}=(a^{11})^{\frac{1}{2}}\bar{u}^{\mathrm{s}}.$$

Therefore, we can write (28) in the relatively simple form

$$\frac{\partial \Gamma}{\partial t}+\frac{1}{r(s)\left[\left(\dfrac{\partial r}{\partial s}\right)^2+\left(\dfrac{\partial z}{\partial s}\right)^2\right]^{\frac{1}{2}}}\left\{\frac{\partial}{\partial s}(\Gamma r(s)\,\bar{u}^{\mathrm{s}})-\frac{1}{P_{\mathrm{s}}}\frac{\partial}{\partial s}\left[\frac{r(s)}{\left[\left(\dfrac{\partial r}{\partial s}\right)^2+\left(\dfrac{\partial z}{\partial s}\right)^2\right]^{\frac{1}{2}}}\frac{\partial \Gamma}{\partial s}\right]\right\}$$
$$+\Gamma(\nabla_{\mathrm{s}}\cdot \boldsymbol{n})\,(\boldsymbol{u}\cdot \boldsymbol{n})=0. \tag{30}$$

This is the proper form of the convective–diffusion equation for transport on the axisymmetric surface, including effects due to the change in shape of the interface with time. In order to solve (30) numerically it is convenient to write it as

$$\frac{\partial \Gamma}{\partial t}+\Lambda_1(s,t)\,\Gamma(s,t)+\Lambda_2(s,t)\frac{\partial \Gamma}{\partial s}+\Lambda_3(s,t)\frac{\partial^2 \Gamma}{\partial s^2}=0, \tag{31}$$

where the coefficients Λ_i depend on the surface velocity, surface shape and the Péclet number.

To actually calculate the surfactant distribution, $\Gamma(s,t+\Delta t)$, we assume, for the moment, that the shape at $t+\Delta t$ and $\Gamma(s,t)$ is known. Then, Γ is discretized using the grid introduced in §4.1 to describe the drop surface, (31) is written in finite-difference form and Γ is assumed to vary quadratically between node points. Therefore, if Γ_i denotes the surfactant concentration at node point i, $\partial\Gamma/\partial s$ and $\partial^2\Gamma/\partial s^2$ at each collocation point can be written in terms of Γ_{i-1}, Γ_i and Γ_{i+1}.

Equation (31) is then written in implicit form at each node point and the tridiagonal linear system of equations that is produced for the surfactant distribution is solved using standard methods. This procedure yields the approximate surfactant distribution at time $t+\Delta t$.

4.3. *Summary of numerical solution scheme*

The problem that we wish to solve numerically consists of the discretized versions of (23), (31) and the kinematic condition (7). The primary difficulty is that these equations are highly coupled. We employ a relatively straightforward, time-marching scheme to solve the problem.

The basic sequence of steps is as follows:

(*a*) For a given shape at time t, calculate the interfacial velocity from (23) and update the shape to time $t+\Delta t$ using (7).

(*b*) Using the known shape at $t+\Delta t$, update the surfactant distribution from $\Gamma(t)$ to $\Gamma(t+\Delta t)$ using (31).

(*c*) Return to (*a*).

This procedure is initiated by beginning with the surfactant uniformly distributed on a spherical shape.

A few additional remarks are necessary to complete and further explain this description of the numerical procedure. The interface shape is updated by integration of the kinematic condition (7) using an explicit Euler method. In order to determine $\Gamma(t+\Delta t)$ on this shape, the convective–diffusion equation (31) is solved using an implicit Euler method as outlined in §4.2. However, because the velocity field corresponding to this new shape is not known, we assume that the velocity field at any node point at $t+\Delta t$ is well-approximated by the velocity at the same node point at time t.† Clearly, this is not exactly correct. However, for the small time steps used in this study, the interface evolves very slowly and this method provides a very good approximation to the convective term in (30). The basic idea is that the evolution of the shape and concentration field from one steady state to another occurs on a long timescale relative to the time step Δt. An obvious improvement of this method would be to use the new velocity field in an iteration scheme to determine the concentration field for a given shape. However, since the explicit/implicit procedure described above is convergent when the (small) time step is decreased (see §5.1) we have not tried to refine it further.

We should add that the same step-wise procedure was used in an attempt to solve the convective–diffusion equation (31) using an explicit Euler method. The numerical solution in this case proved to be very unstable. Using the implicit procedure provided a very stable and smooth solution.

Steady-states solutions are calculated by marching along until the normal velocity is very small (typically $|\boldsymbol{u}\cdot\boldsymbol{n}| < 2\times10^{-4}$) at each collocation point and the surface concentration at any node point changes by a negligible amount between two time steps (typically changes in Γ at a fixed s are less than 10^{-5}). Typically, we choose $N = 15$–20 node points and a time step $\Delta t = 0.0002$–0.005. The numerical procedure can be monitored as time progresses by following the change in volume of the drop and the change in the total amount of surfactant, which must remain constant for the case of an insoluble surfactant. Typically, volume changes are less than one percent for several thousand iterations. Changes in the total amount of surfactant

† Because a normalized measure of arclength is used to describe the surface, and node points are always maintained evenly redistributed, throughout the calculation node points correspond to the same value of the normalized surface coordinate.

are about one percent every thousand iterations and, consequently, after each time step the local surfactant concentration is rescaled in order to maintain the total amount of surfactant constant. Similar difficulties and corrections have been used by previous researchers.

5. Results

In this section we discuss the numerical simulations performed in order to characterize the effects of surfactants on drop deformation in extensional flow fields. The results indicate that the numerical procedure described in §4 can resolve finite deformation and the evolution of the surfactant concentration, both features which are necessary for improved physical insight into the drop breakup process.

5.1. *Convergence of the numerical method*

The numerical method has been tested by (i) decreasing the magnitude of the time step and comparing the calculated steady-state shapes and surfactant concentration distributions at different capillary numbers and (ii) comparing the numerical calculations with the analytical results presented in §3.

First, we consider convergence of the numerical scheme by decreasing the magnitude of the time step. In all cases, for the small time steps used here, the results obtained using one value of the time step are identical with the results obtained when this value is halved. For example, in figure 2, we show the steady-state drop deformation D as a function of the capillary number $\mathbb{C}^*$ for the case $\beta = 0.5$ and $\gamma = 10$. The open squares are the numerical results using a time step $\Delta t = 0.001$ and incrementing the capillary number between steady states by $\Delta\mathbb{C}^* = 0.01$; the crosses are the numerical results with $\Delta t = 0.002$ and $\Delta\mathbb{C}^* = 0.02$. In both simulations the numerical procedure smoothly approaches the same sequence of steady shapes. Also, the concentration profiles at the same stages of the deformation are identical. These results are typical of the numerical simulations for the parameter range studied in this paper.

The predictions of the small-deformation analysis, valid only for small Péclet and capillary numbers, are shown as the symbols in figure 3(a, b), relative to the numerically calculated solid curves. A detailed discussion of these figures is delayed until §5.3. Here, we simply note that the analytical results are only useful for very small distortions and underpredict the finite-deformation results. This feature of the small-deformation analysis severely limits quantitative predictions with regard to finite deformation and possible breakup.

With the level of accuracy discussed above, we use the numerical method in §§5.2–5.5 to examine the effects of β, γ and $\mathbb{C}^*$ on finite drop deformation.

5.2. *An overview of the competing physical processes*

Since a proper account of drop deformation and breakup in the presence of surfactants requires an understanding of coupled, competing effects, we are taking the unusual approach of briefly presenting our conclusions prior to discussing the numerical results. The two principal competing effects associated with surfactant changing the interfacial tension relative to the uniform equilibrium value σ^* are: (i) *convection* of surfactant, previously indicated in the small-deformation analysis, which lowers σ near the end, so tends to produce larger distortions and (ii) *dilution* of surfactant due to increasing interfacial area of the deformed drop. This latter effect increases σ, and so acts opposite the convective transport of surfactant.

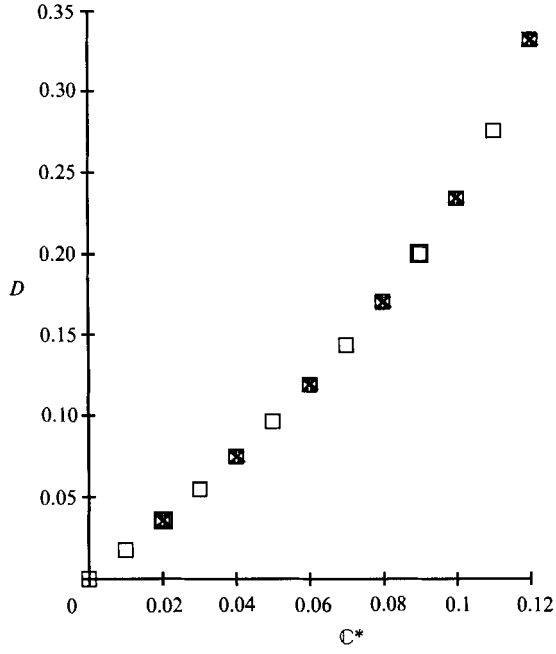

FIGURE 2. Testing of the numerical procedure. Effect of decreasing the time step from 0.002 (x) to 0.001 (□) and simultaneously changing the increment in capillary number from 0.02 (x) to 0.01 (□). The numerical scheme converges to the same sequence of steady shapes. $\beta = 0.5$, $\gamma = 10$.

The influence of surfactants for a fixed value of $\mathbb{C}^*$ depends on the two parameters, β and γ. As an example of the complicated interplay that may occur consider effects associated with variations of β. The parameter β provides a measure of the sensitivity of σ to changes in surfactant concentration so that increasing β for a fixed distribution of surfactant leads to larger interfacial tension gradients. This, in turn, produces lower interfacial tension near the end of the drop, which suggests larger distortions. Nevertheless, for finite deformations, we observe two further coupled responses associated with increasing tangential stresses: (i) as mentioned above, increases of interfacial area dilute the surfactant and increase σ, hence tending to counteract decreases in σ produced by the convective effects; (ii) increased interfacial tension gradients inhibit surface advection and, consequently, surface diffusion acts to produce a more uniform surfactant distribution, a response that also acts to counter the convective effects. In other words, owing to tangential stresses, the effective surface Péclet number is actually decreased by an increase in β even though $P_s = \gamma\mathbb{C}^*$ is held constant.

In a similar manner, increases in γ for fixed β increase the surface Péclet number so that larger surfactant gradients result. Again, this response is counteracted by dilution and Marangoni inhibition (the tangential stresses) of surface transport. In the remaining sections we illustrate these competing influences of surfactants on the drop breakup problem.

5.3. *Evolution of the drop shape and concentration profiles.*

We begin this discussion of the numerical results by presenting typical steady deformation results, D versus $\mathbb{C}^*$, for several combinations of γ and β. A systematic study, varying γ for fixed β, or varying β for fixed γ, will be summarized in §5.4. In

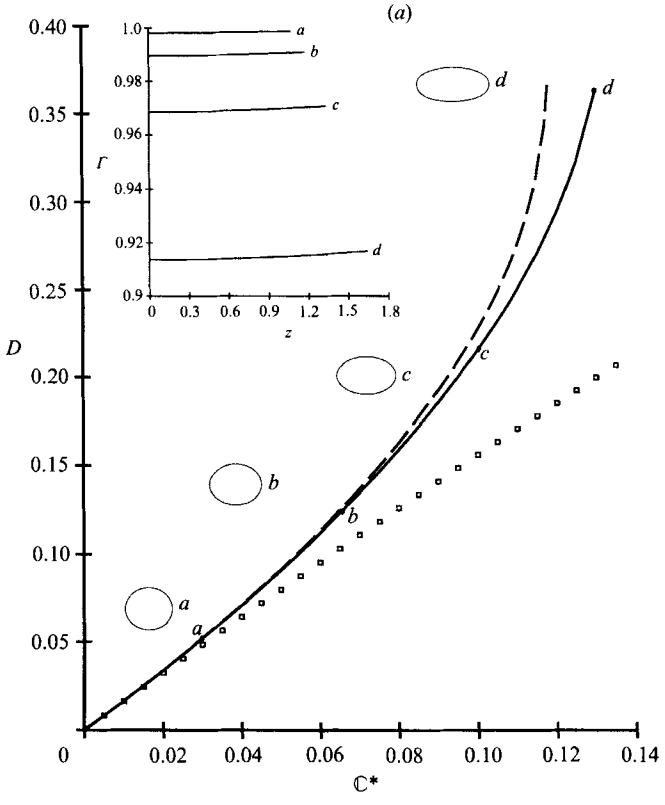
(a)
D
C*
Γ
z
a
b
c
d

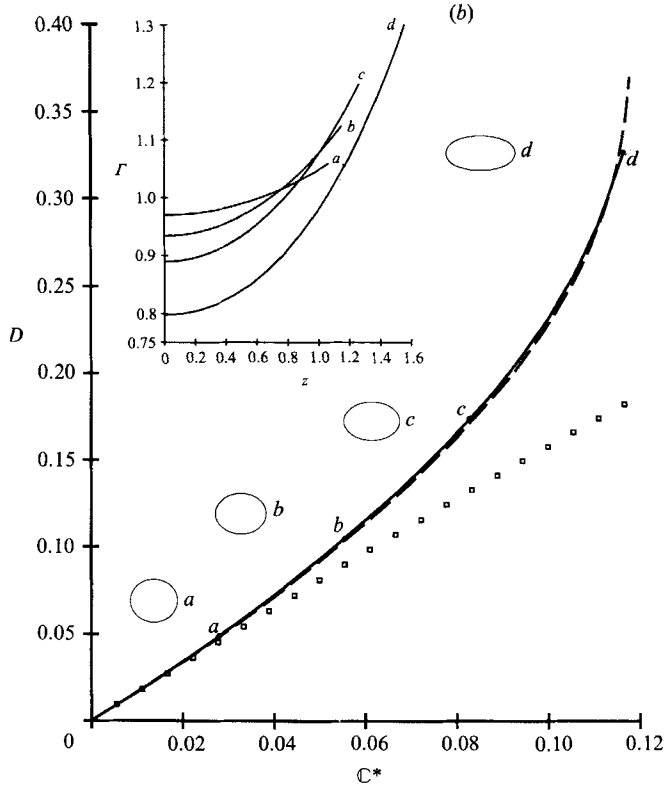
(b)
D
C*
Γ
z
a
b
c
d

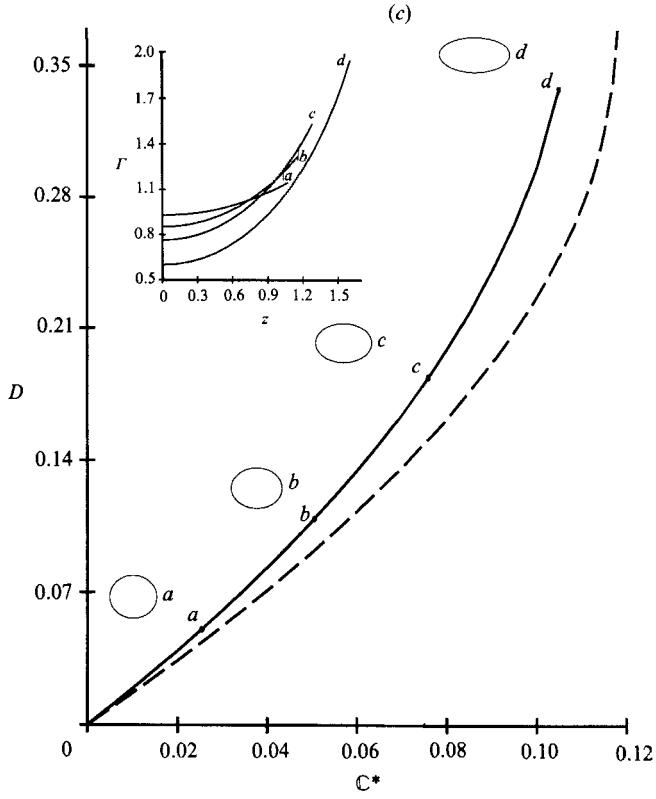

FIGURE 3. Steady-state deformation D as a function of capillary number. (*a*) $\gamma = 0.1$, $\beta = 0.5$; (*b*) $\gamma = 10$, $\beta = 0.1$; (*c*) $\gamma = 1000$, $\beta = 0.3$. The solid line is the numerical calculation with surfactant present and the dashed line is the same drop with the interfacial tension maintained at its initial equilibrium level. The symbols denote the small-deformation prediction. The inset illustrates the surfactant concentration profile Γ as a function of axial position z at intermediate stages of the deformation.

figure 3(*a–c*) we illustrate the drop shape evolution for (*a*) $\gamma = 0.1$, $\beta = 0.5$, (*b*) $\gamma = 10$, $\beta = 0.1$ and (*c*) $\gamma = 1000$, $\beta = 0.3$. The symbols denote the predictions of the small-deformation analysis, the solid lines are the numerical calculations with surfactant and the dashed lines are the same drop, but with the surface tension maintained at the initial equilibrium value. Clearly, differences between the solid and dashed lines represent the combination of effects due to flow-induced dilution and surfactant gradients. The numerical calculations are carried out by incrementing the capillary number until no steady shape exists and the drop undergoes a continuous stretching motion. Also shown in figure 3 are several numerically generated drop shapes. The inset to each of the figures illustrates the evolution of the surfactant concentration profile, presented as concentration Γ versus axial position z along the drop, at intermediate stages of the deformation process. Finally, recall that a simulation holding γ, β fixed and increasing $\mathbb{C}^*$ physically corresponds to an experiment where the shear rate is increased incrementally in a quasi-steady manner. The Péclet number for these simulations is $P_s = \gamma\mathbb{C}^*$ so, in principle, increasing $\mathbb{C}^*$ is equivalent to increasing the importance of convection relative to surface diffusion as the deformation process proceeds. (Nevertheless, as discussed in §5.2, it is important to remember that increasing P_s tends to increase surfactant gradients, thereby

increasing the tangential stresses, which decreases surface velocities, so that the effective Péclet number for surface transport may not increase as quickly as simple estimates would suggest.)

In figure 3(*a*), $\gamma = 0.1$, $\beta = 0.5$, the Péclet number remains small ($< 10^{-2}$) throughout the calculation and, as shown by the inset, the dominance of surface diffusion has the effect of maintaining a nearly uniform surfactant distribution along the interface. Hence, as the drop is distorted by the flow with a consequent increase in interfacial area, the surfactant is diluted, the surfactant concentration decreases and the interfacial tension increases. For the largest steady deformations achieved, the surfactant concentration has decreased almost 10% from its uniform initial value, and this corresponds to $\approx 10\%$ increase in the interfacial tension. This, in turn, requires a 10% increase in shear rate to produce the same deformation as would be obtained for the drop with a uniform distribution of surfactant at the initial equilibrium concentration. This fact explains the larger critical value of the capillary number that is necessary to reach the unsteady stretching mode, $\mathbb{C}_c^* \approx 0.13$.

Since the surfactant concentration remains uniform for this case, the only difference between the two sets of numerical results is a shift in the effective capillary number due to the increase in interfacial tension, relative to the initial equilibrium value, associated with the increase in surface area. Thus, the drop shapes at any fixed value of D are identical and this includes the maximum steady deformation at the critical capillary number. Hence, for the diffusion-dominated regime at low surface Péclet numbers (and $\beta < 0.5$), the interaction between the surfactant and the flow leads to an increase in the critical capillary number for breakup $\mathbb{C}_c^*$ relative to the value that would be predicted based upon the initial equilibrium value of σ^*, and in this sense the presence of insoluble surfactant may be viewed as stabilizing for drop breakup. It must be remembered, however, that the addition of surfactant leads to a large decrease in the equilibrium value of σ^* relative to the interfacial tension for a clean interface, and the critical strain rate for breakup will still be decreased by a large amount compared to its value with no surfactant present. It should also be noted that as β is increased further, more extended steady shapes become possible owing to the existence of significant tangential Marangoni stresses (e.g. see (14)), thus substantially increasing the dilution effect and the critical capillary number for breakup (see figure 6).

The case of $P_s \approx 1$ is considered in figure 3(*b*) for $\gamma = 10$, $\beta = 0.1$. As the Péclet number is now $O(1)$ throughout most of the deformation process, large variations in surfactant concentration occur between the end and the centre of the drop (see inset). For the largest steady deformation calculated, the surfactant concentration is about 30% higher at the end than the initial value. In general, these surfactant gradients would be expected to lead to significant variations in interfacial tension, and thus to discernable differences in drop shape and the dependence of deformation on $\mathbb{C}^*$. However, in this simulation, β is small, and the changes in surface tension are only about 3% relative to the initial value for the uniformly contaminated surface. As a consequence, the deformation curve and the critical capillary number necessary to produce unsteady stretching associated with the first stages of drop breakup are indistinguishable from the uniformly contaminated case shown as the dashed line. Later, we shall see that significant differences will become apparent at the same value of γ, but larger values of β.

The final case illustrated, figure 3(*c*), shows typical results when γ is large so that the Péclet number is effectively $O(100)$ throughout most of the deformation process. In this figure the numerically calculated deformation curve clearly indicates a

significantly larger deformation than the equivalent drop with a uniform surfactant distribution at the initial equilibrium level. The increased deformation is simply due to large convective effects transporting surfactant toward the end of the drop, thereby lowering interfacial tension, hence requiring increased deformation to satisfy the normal stress balance. This influence of surfactants was suggested by the small-deformation analysis of §3. Comparing the two curves in figure 3(*c*), the influence of surface tension gradients has decreased the critical capillary number for breakup by about 10%, even though the interfacial tension near the end is more than 15% below its initial value on the spherical drop. Finally, we note that Smith & van de Ven (1985) observe greater drop deformation in shear flows when surfactants are present, relative to the uniform interfacial tension case, which is in qualitative agreement with the large-γ numerical calculations reported here.

5.4. *The effects of γ and β*

In this section, we present the results from a systematic investigation varying the physicochemical parameter β for fixed values of γ and varying γ for fixed values of β. Once again we show curves of D versus $\mathbb{C}^*$, continued until the drop begins to undergo a continuous extension characteristic of the first stages of drop breakup. It is difficult to make general statements about the independent influences of β, γ since both parameters affect the magnitude of the tangential stress gradients. This in turn affects the magnitude of the interfacial velocity which is, of course, coupled with the tangential stress variations since the interfacial velocity determines the relative magnitude of convection to diffusion along the interface. Nevertheless, several trends concerning drop breakup are identified as were discussed in §5.2.

The influence due to variation of the physicochemical parameter β for fixed values of $\gamma = 10$ and 1000 is examined in figures 4(*a*), and 4(*b*), respectively. The inset illustrates the concentration distribution as a function of axial position for the most highly deformed steady drop shapes calculated. For lower values of γ, say $\gamma < 0.1$, the surface Péclet number remains small for the values of capillary number representative of drop deformation in uniaxial extensional flows and the surfactant remains uniformly distributed. In such instances, at least for small β, the primary effect of surfactant is to modify the interfacial tension, and the critical capillary number for breakup may be predicted from the clean interface calculations, with account taken of the dilution factor due to increased surface area as the drop is deformed, as discussed for figure 3(*a*) (see also figure 6).

In figure 4(*a*), $\gamma = 10$, we observe that the maximum steady deformation increases with increasing β. For large β values ($\beta > 0.5$), we further observe that because of the interfacial area increase, and in spite of the convective effects, the surfactant is diluted so that the surfactant concentration everywhere along the interface is eventually lower than the initial concentration. Hence, this dilution leads to larger interfacial tensions than present on the initial spherical drop and the critical capillary number increases beyond naïve estimates of breakup based on the interfacial tension of the uniformly coated spherical surface. We also observe that a related role of the existence of tangential stresses and surfactant gradients is to allow highly deformed steady shapes, $D \approx 0.5$; such large distortions are only observed in the absence of surfactants if the viscosity of the droplet is much lower than the suspending-fluid viscosity.

In figure 4(*b*), $\gamma = 1000$, the behaviour is similar. These simulations correspond, at least in principle, to large surface Péclet numbers. The curve labelled (*a*) shows that low values of β lead to significant variations in surface concentration, from almost

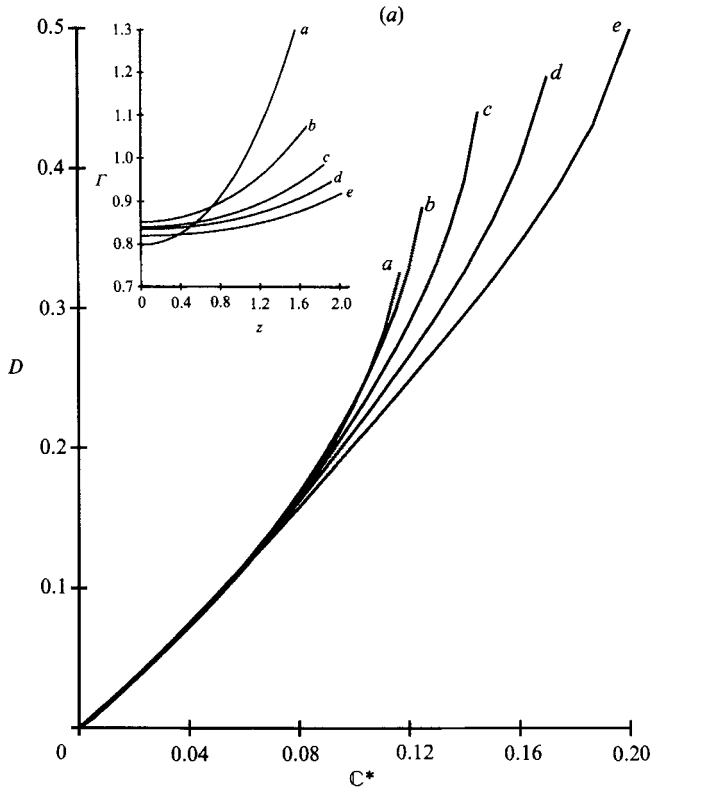
(a)
D
C*
Γ
z
a
b
c
d
e

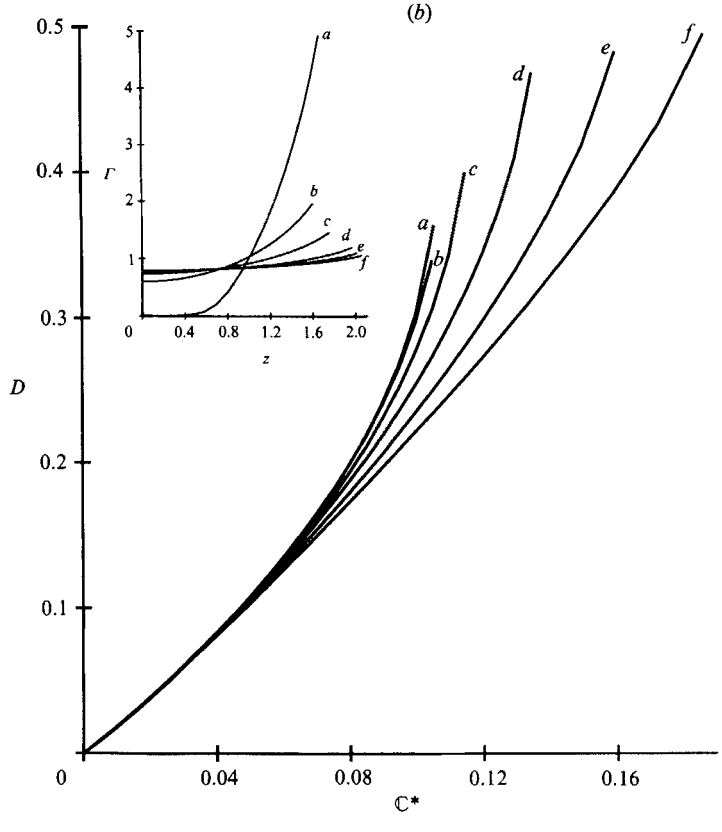
(b)
D
C*
Γ
z
a
b
c
d
e
f

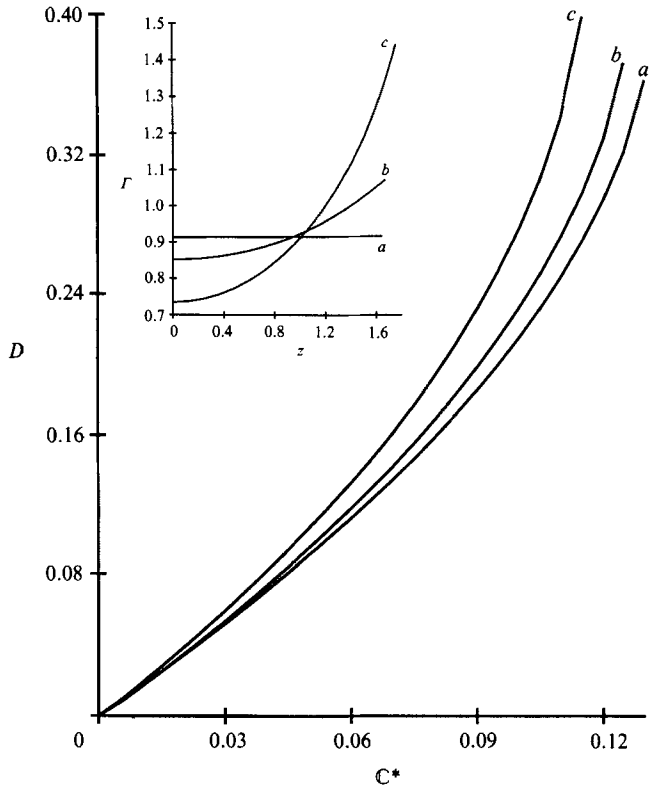

FIGURE 5. The result of varying γ for a fixed value of $\beta = 0.5$. Curves a–c correspond to $\gamma = 0.1$, 10, 1000, respectively. The inset illustrates the concentration profiles for the most highly deformed steady shapes calculated.

zero near the drop midsection to $\Gamma \approx 5$ near the end of the drop. The curves for $\beta = 0.1, 0.3$, are practically indistinguishable and breakup occurs at approximately the same $\mathbb{C}^*$, D, which, as we saw in figure 3(c), is at a slightly lower capillary number than the same drop maintained at its initial interfacial tension. This is a direct consequence of convection of surfactant producing low interfacial tensions near the end of the drop; indeed, interfacial tensions are lower than their initial value over almost half of the drop surface. However, further increases in β lead to more uniform surfactant distributions, large steady deformations and also substantial increases are observed in the critical capillary number necessary for breakup.

In both figures 4(a) and 4(b) we observe that, as β increases, the gradient in the surfactant concentration near the end of the drop decreases substantially. For $\beta > 0.5$, even in the case of large γ, there is only a small difference between the concentration at the end of the drop and the concentration along the drop midsection. On the other hand, for small β and large γ, figure 4(b), we see very large concentration variations near the end of the drop, as a surfactant concentration boundary layer forms due to the large convective effects.

Finally, in figure 5 we examine the results typical of variations in γ at a fixed value of $\beta = 0.5$. Qualitatively, these results are typical of other values of β. Once again,

FIGURE 4. The result of varying β for fixed values of γ. (a) $\gamma = 10$; curves a–e correspond to $\beta = 0.1, 0.5, 0.7, 0.8, 0.85$, respectively; ($b$) $\gamma = 1000$; curves a–f correspond to $\beta = 0.1, 0.3, 0.5, 0.7, 0.8, 0.85$, respectively. The inset illustrates the concentration profiles for the most highly deformed steady shapes calculated.

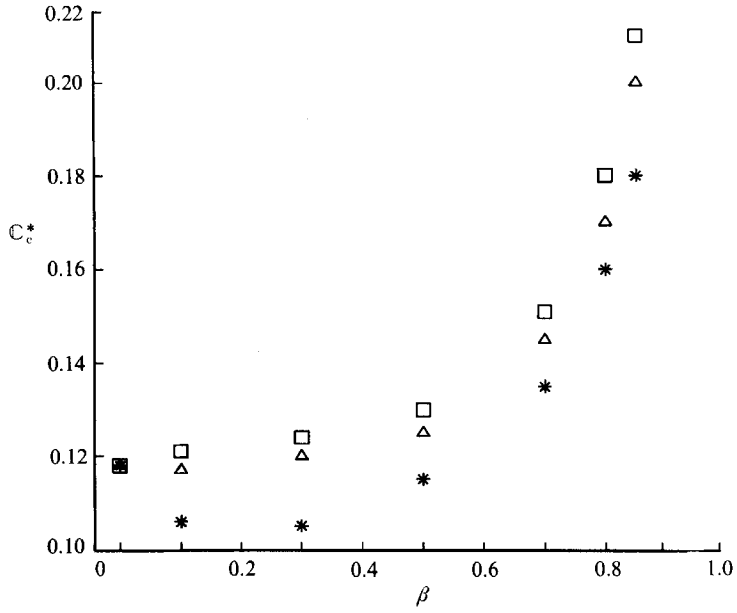

FIGURE 6. Critical capillary number $\mathbb{C}_c^*$ as a function of β for different γ: □, $\gamma = 0.1$; △, $\gamma = 10$; *, $\gamma = 1000$. Note that the critical capillary number for the equivalent drop maintained at its initial equilibrium interfacial tension is $\mathbb{C}_c^* \approx 0.12$.

the inset illustrates the concentration profile for the most highly deformed steady shapes calculated. This set of simulations corresponds to decreasing the surface diffusivity while maintaining all other parameters constant. It is clear from figure 5 that as the surface diffusivity is decreased (γ increases), the surfactant is swept to the end, lowering interfacial tension and consequently increasing deformation. Hence, all other parameters remaining fixed, the critical capillary number for breakup decreases as γ increases.

5.5. *Critical capillary number for breakup*

We conclude our discussion by illustrating the critical capillary number for breakup (i.e. non-existence of a steady drop shape), $\mathbb{C}_c^*$, as a function of β and γ. The results shown in figure 6 are for $0 \leqslant \beta \leqslant 0.85$ and $0.1 \leqslant \gamma \leqslant 1000$ and summarize much of the previous discussion, at least insofar as the overall effects of β, γ on the critical shear rate are concerned. We remind the reader that the critical capillary number includes the decrease in interfacial tension due to the presence of surfactant at the uniform equilibrium concentration, $\Gamma = 1$.

We see that for $\beta < 0.5$ there is only a small variation in $\mathbb{C}_c^*$ relative to the value at $\beta = 0$. In this small-β regime, the lower interfacial tension produced by the higher surfactant concentrations at the end of the drop are roughly offset by dilution of surfactant. For small γ there is actually a small increase in $\mathbb{C}_c^*$ due to the dilution of the surfactant as the drop deforms and for large γ there is a small decrease in $\mathbb{C}_c^*$ due to the convective effect.

As β is increased above 0.5, we previously observed dilution of the surfactant to concentration levels below the initial concentration and this effect is even more pronounced since the complicated response to tangential stresses leads to large steady deformations. The increased values of the interfacial tension accompanying dilution lead to the sharp increase in $\mathbb{C}_c^*$ shown in figure 6. We also clearly see that

for any β, the critical capillary number for breakup is lower as γ is increased (see figure 5).

6. Conclusions

In this paper we have examined drop deformation in extensional flows in the presence of insoluble surface-active agents. The analytical results are useful conceptually, but of limited practical value since they are restricted to small deformations. An approximate numerical scheme based on the boundary-integral method has been developed that is capable of analysing this time-dependent, coupled free-boundary/surfactant transport problem. The numerical simulations of finite deformation suggest that the two important, competing processes are convection of surfactant, which lowers interfacial tension and hence increases deformation (in agreement with an experimental observation of Smith & van de Ven), and dilution of the surfactant due to the increase of interfacial area that accompanies drop deformation. From the standpoint of breakup, for $\beta < 0.5$ there is only a small variation in the critical capillary number $\mathbb{C}_c^*$ over all γ values studied. However, significant increases in $\mathbb{C}_c^*$ are shown in figure 6 as β increases, owing to increased tangential stresses, larger steady deformations and the accompanying dilution of surfactant.

H.A.S. would like to thank Drs E. J. Hinch and Ali Nadim for several helpful discussions regarding this problem. We also thank Professor Avinoam Nir for providing us with preprints of his work. Initial stages of this work were supported by IBM through a Graduate Research Fellowship to H.A.S. and by a grant to L.G.L. from the fluid mechanics program of the National Science Foundation. The final stages of this work were supported by a NSF grant to H.A.S. All of the above support is gratefully appreciated.

Appendix

In this Appendix we describe the solution to the time-dependent small deformation of a drop in a steady linear straining flow. The governing equations and boundary conditions were presented in §2. For the linear flow field $\boldsymbol{u}_\infty = \frac{1}{2}\boldsymbol{\omega} \wedge \boldsymbol{x} + \boldsymbol{E}\cdot\boldsymbol{x}$, the first corrections to the description of the nearly spherical surface shape and the surfactant distribution (assumed nearly uniform) are expected to be of the form

$$r = 1 + \mathbb{C}^* b_r(t) \frac{\boldsymbol{x}\cdot\boldsymbol{E}\cdot\boldsymbol{x}}{r^2}, \tag{A 1}$$

$$\Gamma = 1 + \gamma\mathbb{C}^* b_\Gamma(t) \frac{\boldsymbol{x}\cdot\boldsymbol{E}\cdot\boldsymbol{x}}{r^2}, \tag{A 2}$$

where $\boldsymbol{E}$ is the rate-of-strain tensor, $\mathbb{C}^* \ll 1$ and $\gamma = O(1)$. The appearance of the small parameter $\mathbb{C}^*$ in (A 1) follows from the normal stress balance, while the appearance of the small parameter $\gamma\mathbb{C}^* = P_s$ in (A 2), representing small surface Péclet numbers, follows from analysis of the surface convective–diffusion equation. As discussed by Rallison (1980), the analysis assumes $\lambda = O(1)$ since for large λ the vorticity terms become important.

If we define the shape function as

$$f = r - \left[1 + \mathbb{C}^* b_r(t) \frac{\boldsymbol{x}\cdot\boldsymbol{E}\cdot\boldsymbol{x}}{r^2}\right] = \text{constant} = 0, \tag{A 3}$$

then the unit outward normal to the (deformed) interface can be calculated from

$$\boldsymbol{n} = \frac{\nabla f}{|\nabla f|}. \tag{A 4}$$

Hence, the local mean curvature of the slightly deformed drop shape is

$$\nabla\cdot\boldsymbol{n} = 2 + 4\mathbb{C}^* b_r(t)\, \boldsymbol{n}^0\cdot\boldsymbol{E}\cdot\boldsymbol{n}^0 \tag{A 5}$$

where $\boldsymbol{n}^0$ denotes the normal to the spherical surface.

Using Lamb's general solution, the velocity and pressure fields internal and external to the spherical drop can be expressed in the general forms

$$\boldsymbol{u}(\boldsymbol{x}) = \tfrac{1}{2}\boldsymbol{\omega}\wedge\boldsymbol{x} + \boldsymbol{E}\cdot\boldsymbol{x} + c_1\frac{\boldsymbol{\omega}\wedge\boldsymbol{x}}{r^3} + \frac{c_2}{r^5}\left[2\boldsymbol{E}\cdot\boldsymbol{x} - 5\boldsymbol{x}\frac{\boldsymbol{x}\cdot\boldsymbol{E}\cdot\boldsymbol{x}}{r^2}\right] + c_3\,\boldsymbol{x}\frac{\boldsymbol{x}\cdot\boldsymbol{E}\cdot\boldsymbol{x}}{r^5}, \tag{A 6}$$

$$p(\boldsymbol{x}) = p_\infty + 2c_3\frac{\boldsymbol{x}\cdot\boldsymbol{E}\cdot\boldsymbol{x}}{r^5}, \tag{A 7}$$

$$\hat{\boldsymbol{u}}(\boldsymbol{x}) = \hat{c}_1\,\boldsymbol{\omega}\wedge\boldsymbol{x} + 2\hat{c}_2\boldsymbol{E}\cdot\boldsymbol{x} + \hat{c}_3[5r^2\boldsymbol{E}\cdot\boldsymbol{x} - 2\boldsymbol{x}\boldsymbol{x}\cdot\boldsymbol{E}\cdot\boldsymbol{x}], \tag{A 8}$$

$$\hat{p}(\boldsymbol{x}) = p_0 + 21\hat{c}_3\,\boldsymbol{x}\cdot\boldsymbol{E}\cdot\boldsymbol{x}. \tag{A 9}$$

For the general time-dependent problem the coefficients $c_1, c_2, c_3, \hat{c}_1, \hat{c}_2, \hat{c}_3$ are functions of time. In order to obtain a leading-order solution for the flow fields, the pressure distributions, the drop shape, and the surfactant distribution, we must apply the boundary conditions from §2. For nearly spherical shapes, we follow the standard procedure of domain perturbations, so that the leading-order solution is determined by evaluating all boundary conditions on the undeformed spherical surface, $r = 1$ and $\boldsymbol{x} = \boldsymbol{n}^0$.

Continuity of velocity $\boldsymbol{u} = \hat{\boldsymbol{u}}$ at the fluid–fluid interface yields

$$1 + 2c_2 = 2\hat{c}_2 + 5\hat{c}_3, \quad -5c_2 + c_3 = -2\hat{c}_3, \quad \tfrac{1}{2} + c_1 = \hat{c}_1. \tag{A 10}$$

Application of the kinematic condition $\boldsymbol{u}\cdot\boldsymbol{n} = \hat{\boldsymbol{u}}\cdot\boldsymbol{n} = \mathrm{d}r/\mathrm{d}t$ at $r = 1$, $\boldsymbol{x} = \boldsymbol{n}^0$ yields

$$1 - 3c_2 + c_3 = 2\hat{c}_2 + 3\hat{c}_3 = \mathbb{C}^*\frac{\mathrm{d}b_r}{\mathrm{d}t}, \tag{A 11}$$

where, following Frankel & Acrivos (1970), we retain the time derivative at this order, thereby assuming $\mathbb{C}^*\,\mathrm{d}b_r/\mathrm{d}t = O(1)$. The tangential stress balance gives

$$2 - 16c_2 + 2c_3 - 4\lambda(\hat{c}_2 + 4\hat{c}_3) = 2\frac{\beta\gamma}{(1-\beta)}b_\Gamma \tag{A 12}$$

and

$$c_1 = 0 \rightarrow \hat{c}_1 = \tfrac{1}{2}. \tag{A 13}$$

The normal stress balance includes both curvature variations (proportional to $\mathbb{C}^*$) and interfacial tension variations (proportional to $\gamma\mathbb{C}^* = P_s$), so that

$$2 + 24c_2 - 6c_3 - \lambda(4\hat{c}_2 - 3\hat{c}_3) = 4b_r - 2\frac{\beta\gamma}{(1-\beta)}b_\Gamma. \tag{A 14}$$

The system of equations is completed by keeping the leading-order terms from the time-dependent surface convective–diffusion equation. If Γ' denotes the deviation from the uniformly coated interface ($\Gamma = 1+\Gamma'$), then at leading order (15) gives

$$\frac{\partial \Gamma'}{\partial t} + \nabla_s \cdot \boldsymbol{u}_s + (\nabla_s \cdot \boldsymbol{n})(\boldsymbol{u}\cdot\boldsymbol{n}) = \frac{1}{\gamma \mathbb{C}^*} \nabla_s^2 \Gamma'. \tag{A 15}$$

Using the above results and keeping all terms $O(\mathbb{C}^*)$ we find that (A 15) yields

$$\gamma \mathbb{C}^* \frac{\mathrm{d}b_\Gamma}{\mathrm{d}t} - (6\hat{c}_2 + 15\hat{c}_3) + 2\mathbb{C}^* \frac{\mathrm{d}b_r}{\mathrm{d}t} = -6b_\Gamma, \tag{A 16}$$

where we again retain time derivatives, which is self-consistent for both short times, $t \sim O(\mathbb{C}^*)$ and long times (provided the deformation remains small). The third term in this equation describes local concentration changes due to the local contraction and stretching of the surface. We now have six equations for the six remaining unknowns. After some tedious algebra, a second-order differential equation is found describing the evolution of $b_r(t)$ (equation (22)) and the steady-state result (equation (19)). Similarly, $b_\Gamma(t)$ satisfies

$$\frac{(2\lambda+3)(19\lambda+16)}{2}\gamma\mathbb{C}^{*2}\frac{\mathrm{d}^2 b_\Gamma}{\mathrm{d}t^2} + \left[3\mathbb{C}^*(2\lambda+3)(19\lambda+16) + (32+23\lambda)\frac{\beta\gamma\mathbb{C}^*}{1-\beta} + 20(1+\lambda)\gamma\mathbb{C}^*\right]\frac{\mathrm{d}b_\Gamma}{\mathrm{d}t} + 24\left[5(1+\lambda)+\frac{\beta\gamma}{1-\beta}\right]b_\Gamma = 60. \tag{A 17}$$

REFERENCES

Acrivos, A. 1983 The breakup of small drops and bubbles in shear flows. *Ann. NY Acad. Sci.* **404**, 1–11.

Adamson, A. W. 1976 *Physical Chemistry of Surfaces*, 3rd edn. John Wiley & Sons.

Aris, R. 1962 *Vectors, Tensors, and the Basic Equations of Fluid Mechanics*. Prentice-Hall.

Ascoli, E. P. & Leal, L. G. 1990 Thermocapillary migration of a deformable drop toward a planar wall. *J. Colloid Interface Sci.* (accepted).

Barthes-Biesel, D. & Acrivos, A. 1973 Deformation and burst of a liquid droplet freely suspended in a linear shear field. *J. Fluid Mech.* **61**, 1–21.

Bentley, B. J. & Leal, L. G. 1986 An experimental investigation of drop deformation and breakup in steady two-dimensional linear flows. *J. Fluid Mech.* **167**, 241–283.

Cox, R. G. 1969 The deformation of a drop in a general time-dependent fluid flow. *J. Fluid Mech.* **37**, 601–623.

Flumerfelt, R. W. 1980 Effects of dynamic interfacial properties on drop deformation and orientation in shear and extensional flow fields. *J. Colloid Interface Sci.* **76**, 330–349.

Frankel, N. A. & Acrivos, A. 1970 The constitutive equation for a dilute emulsion. *J. Fluid Mech.* **44**, 65–78.

Greenspan, H. P. 1978 On fluid-mechanical simulations of cell division and movement. *J. Theor. Biol.* **70**, 125–134.

Haber, S. & Hetsroni, G. 1971 Hydrodynamics of a drop submerged in an unbounded arbitrary velocity field in the presence of surfactants. *Appl. Sci. Res.* **25**, 215–233.

Holbrook, J. A. & LeVan, M. D. 1983*a* Retardation of droplet motion by surfactant. Part 1. Theoretical development and asymptotic solutions. *Chem. Engng Commun.* **20**, 191–207.

Holbrook, J. A. & LeVan, M. D. 1983*b* Retardation of droplet motion by surfactant. Part 2. Numerical solutions for exterior diffusion, surface diffusion, and adsorption kinetics. *Chem. Engng Commun.* **20**, 273–290.

LEE, S. H. & LEAL, L. G. 1982 The motion of a sphere in the presence of a deformable interface. II. A numerical study of the translation of a sphere normal to an interface. *J. Colloid Interface Sci.* **87**, 81–106.

LEVAN, M. D. & NEWMAN, J. 1976 The effect of surfactant on the terminal and interfacial velocities of a bubble or drop. *AIChE J.* **22**, 695–701.

LEVICH, V. G. 1962 *Physicochemical Hydrodynamics.* Prentice-Hall.

LEVICH, V. G. & KRYLOV, V. S. 1958 Surface-tension-driven phenomena. *Ann. Rev. Fluid Mech.* **1**, 293–316.

LI, X. Z., BARTHES-BIESEL, X. X. & HELMY, A. 1988 Large deformations and burst of a capsule freely suspended in an elongational flow. *J. Fluid Mech.* **187**, 179–196.

MCCONNELL, A. J. 1957 *Applications of Tensor Analysis.* Dover.

NEWMAN, J. 1967 Retardation of falling drops. *Chem. Engng Sci.* **22**, 83–85.

PHILLIPS, W. J., GRAVES, R. W. & FLUMERFELT, R. W. 1980 Experimental studies of drop dynamics in shear fields: Role of dynamic interfacial effects. *J. Colloid Interface Sci.* **76**, 350–370.

RALLISON, J. M. 1980 A note on the time-dependent deformation of a viscous drop which is almost spherical. *J. Fluid Mech.* **98**, 625–633.

RALLISON, J. M. 1981 A numerical study of the deformation and burst of a viscous drop in general shear flows. *J. Fluid Mech.* **109**, 465–482.

RALLISON, J. M. 1984 The deformation of small viscous drops and bubbles in shear flows. *Ann. Rev. Fluid Mech.* **16**, 45–66.

RALLISON, J. M. & ACRIVOS, A. 1978 A numerical study of the deformation and burst of a viscous drop in general shear flows. *J. Fluid Mech.* **89**, 191–200.

RUMSCHEIDT, F. D. & MASON, S. G. 1961 Particle motions in sheared suspensions XII. Deformation and burst of fluid drops in shear and hyperbolic flow. *J. Colloid Sci.* **16**, 238–261.

SADHAL, S. S. & JOHNSON, R. E. 1986 On the deformation of drops and bubbles with varying interfacial tension. *Chem. Engng Commun.* **46**, 97–109.

SAVILLE, D. A. 1973 The effect of interfacial tension gradients on the motion of drops and bubbles. *Chem. Engng J.* **5**, 251–259.

SHERWOOD, J. D. 1988 Breakup of fluid droplets in electric and magnetic fields. *J. Fluid Mech.* **188**, 133–146.

SMITH, P. G. & VEN, T. G. M. VAN DE 1985 Shear-induced deformation and rupture of suspended solid/liquid clusters. *Colloids and Surfaces* **15**, 191–210.

STONE, H. A. 1990 A simple derivation of the time-dependent convective–diffusion equation for surfactant transport along a deforming interface. *Phys. Fluids* A **2**, 111–112.

STONE, H. A., BENTLEY, B. J. & LEAL, L. G. 1986 An experimental study of transient effects in the breakup of viscous drops. *J. Fluid Mech.* **173**, 131–158.

STONE, H. A. & LEAL, L. G. 1989 Relaxation and breakup of an initially extended drop in an otherwise quiescent fluid. *J. Fluid Mech.* **198**, 399–427.

STOOS, J. A. & LEAL, L. G. 1989 Particle motion in axisymmetric stagnation flow toward an interface. *AIChE J.* **35**, 196–212.

TAYLOR, G. I. 1932 The viscosity of a fluid containing small drops of another fluid. *Proc. R. Soc. Lond.* A **138**, 41–48.

TAYLOR, G. I. 1934 The formation of emulsions in definable fields of flow. *Proc. R. Soc. Lond.* A **146**, 501–523.

TORZA, S., COX, R. G. & MASON, S. G. 1972 Particle motions in sheared suspensions. XXVII. Transient and steady deformation and burst of liquid drops. *J. Colloid Interface Sci.* **38**, 395–411.

WAXMAN, A. M. 1984 Dynamics of a couple-stress fluid membrane. *Stud. Appl. Maths* **70**, 63–86.

ZINEMANAS, D. & NIR, A. 1988 On the viscous deformation of biological cells under anisotropic surface tension. *J. Fluid Mech.* **193**, 217–241.